Luminescence studies and EPR investigation of solution combustion derived Eu doped ZnO

A. JagannathaReddy, M.K. Kokila, H. Nagabhushana, C. Shivakumara, R.P.S. Chakradhar, B.M. Nagabhushana, R. Hari Krishna

PII: S1386-1425(14)00637-4
DOI: http://dx.doi.org/10.1016/j.saa.2014.04.064
Reference: SAA 12028

To appear in: *Spectrochimica Acta Part A: Molecular and Biomolecular Spectroscopy*

Received Date: 8 October 2013
Revised Date: 11 March 2014
Accepted Date: 13 April 2014

Please cite this article as: A. JagannathaReddy, M.K. Kokila, H. Nagabhushana, C. Shivakumara, R.P.S. Chakradhar, B.M. Nagabhushana, R. Hari Krishna, Luminescence studies and EPR investigation of solution combustion derived Eu doped ZnO, *Spectrochimica Acta Part A: Molecular and Biomolecular Spectroscopy* (2014), doi: http://dx.doi.org/10.1016/j.saa.2014.04.064

Luminescence studies and EPR investigation of solution combustion derived Eu doped ZnO

A. JagannathaReddy[a*], M. K. Kokila[b], H. Nagabhushana[c], C. Shivakumara[d], R. P. S. Chakradhar[e], B.M. Nagabhushana[f], R. Hari Krishna[f*]

[a]*Department of Physics, M. S. Ramaiah Institute of Technology, Bangalore – 560 054, India.*
[b]*Department of Physics, Bangalore University, Bangalore – 560 056,India.*
[c]*Centre for Advanced Materials Research, Tumkur University, Tumkur - 572 103, India.*
[d]*Solid State and Structural Chemistry Unit, Indian Institute of Science, Bangalore -560 012, India.*
[e]*National Aerospace Laboratories (CSIR), Bangalore-56017, India.*
[f]*Department of Chemistry, M. S. Ramaiah Institute of Technology, Bangalore – 560 054, India.*

Abstract

ZnO:Eu (0.1 mol%) nanopowders have been synthesized by auto ignition based low temperature solution combustion method. Powder X-ray diffraction (PXRD) patterns confirm the nano sized particles which exhibit hexagonal wurtzite structure. The crystallite size estimated from Scherrer's formula was found to be in the range ~ 35-39 nm. Scanning electron microscopy (SEM) and transmission electron microscopy (TEM) studies reveal particles are agglomerated with quasi-hexagonal morphology. A blue shift of absorption edge with increase in band gap is observed for Eu doped ZnO samples. Upon 254 nm excitation, ZnO:Eunanopowders show peaks in regions blue (420-484 nm), green (528 nm) and red (600 nm) which corresponds to both Eu^{2+} and Eu^{3+} ions. The Electron paramagnetic resonance (EPR) spectrum exhibits a broad resonance signal at g = 4.195 which is attributed to Eu^{2+} ions. Further, EPR and thermoluminescence (TL) studies reveal presence of native defects in this phosphor. Using TL glow peaks the trap parameters have been evaluated and discussed.

Keywords: ZnO; nanopowder; photoluminescence; EPR; Thermoluminescence

* Corresponding author: ajreddy09@gmail.com (A. Jagannatha Reddy)
Tel.: +91 9886537250 (M) rhk.chem@gmail.com (R. Hari Krishna)

1. Introduction

Recently, rare-earth (RE) doped II-VI semiconductors have received significant attention due to their applications in optoelectronic devices [1- 5]. The rare earth activated oxide phosphors have good luminescent characteristics, stability in high vacuum, and absence of corrosive gas emission under electron bombardment when compared to currently used sulfide based phosphors. Trivalent RE^{3+} ions exhibit very sharp and temperature independent RE intra-4f shell transitions, since the 4f shell is well shielded by the outer 5s and 5p electrons.The red-emitting phosphors doped with trivalent RE^{3+} ions have been widely used in the development of emissive display and tricolor lamp industry.

Europium ion is usually a good choice for many luminescent applications because trivalent europium (Eu^{3+}) is an excellent red activator while divalent europium (Eu^{2+}) can provide efficient blue or green emission under near-ultraviolet excitation.The red $^5D_0$–$^7F_2$ emission of Eu^{3+} is widely explored in light-emitting devices. The luminescence properties of Eu^{2+} ions activated materials have been investigated for a long time as efficient blue or green emission in many kinds of commercial phosphors [6–7].

The use of a semiconductor host enables minority carrier injection to excite RE 4f shell electrons, resulting in 4f shell luminescence. ZnO is a well known direct wide band gap II-VI semiconductor (3.37 eV) which is economical, environmental friendly, and exhibits high thermal and chemical stability [1,5]. Importantly, it has a large exciton binding energy of 60 meV which is much higher than the thermal energy at room temperature (RT). These properties make ZnO a unique host material for doping with luminescence centers and it can exhibit efficient emission even at or above RT.

ZnO nanostructures have been prepared by several workers employing various synthesis methods such as precipitation [8], spray pyrolysis [9], chemical bath deposition [10], thermal decomposition [11], hydrothermal synthesis [12], sol–gel [13], solid-state pyrolytic reactions [14]. Solid-state reactions are performed at high temperatures, typically ~1600 ^{0}C, because of the refractory nature of the oxide precursors while in sol–gel and precipitation methods, dilute solutions of metal organics or metal salts are reacted and condensed into an amorphous or weakly crystalline mass. Hydrothermal synthesis is a low temperature and high pressure decomposition technique that produces fine, well-crystallized powders. However, the solid state and sol-gel methods require long processing time and also as-synthesized materials must be heat treated to high temperatures to crystallize the desired phase. Combustion synthesis is a novel technique that has been applied to phosphor synthesis in the past few years. This technique produces highly crystalline powders in the as-synthesized state. The synthesized powders are generally more homogeneous, have fewer impurities, and have higher surface area than other conventional solid-state methods.

As a part of our programme on nanomaterials, here we report Europium (Eu) activated Zinc oxide nanoparticles prepared by a simple low temperature solution combustion route. The nanopowders are well characterized using different spectroscopy techniques. Electron paramagnetic resonance (EPR), photoluminescence (PL) and thermoluminescence (TL) studies of these phosphors are carried out. In the last few years, TL of ZnO nanostructures have been investigated by several researchers using beta (β) and X-ray irradiation [15-17]. However, TL studies on ZnO:Eu nanopowders with γ-

irradiation are scarce as evident from the literature. Therefore, the present paper intends to investigate the TL properties of γ- irradiated ZnO:Eunanopowders.

2. Experimental

2.1. Synthesis

Nano-crystalline ZnOhas been prepared using zinc nitrate [$Zn(NO_3)_2$] as oxidiser and oxalyl di-hydrazide (ODH) as fuel at a relatively lower temperature (300 ^oC). The stoichiometry of the redox mixture for combustion is calculated on the total oxidizing and reducing valencies of the oxidizer and the fuel using the concept of propellant chemistry [18]. In undoped ZnO sample preparation, zinc nitrate (5.0 g) and ODH (1.98 g) were dissolved in minimum quantity of double distilled water and heated on a hot plate. The homogeneous solution so obtained is taken in a cylindrical Petri dish and introduced into a muffle furnace maintained at 300 ±10^oC. The solution boils, dehydrates, and ruptures into a flame within 5min. Combustion occurred instantaneously leading to flame type of combustion. The resultant product is a voluminous, foamy powder which occupies the entire volume of the reaction vessel. The white ZnO nano product was collected. For safety, the preparation was performed inside a fume hood. Similarly 0.1 mol% Eu doped ZnO sample was prepared by taking 0.00298 g of Europium oxide (Eu_2O_3) which was converted in to europium nitrate by dissolving it with (1:1) HNO_3 and heated on sand bath until excess nitric acid evaporates. For this, 5.0 g of $Zn(NO_3)_2$, 1.98 g of ODH fuel and double distilled water are added and stirred for 5 minutes using magnetic stirrer and combustion was carried out as mentioned above. Theoretical equation assuming complete combustion of the redox mixture used for the synthesis of doped ZnO may be written as

$$Zn(NO_3)_2 + xEu(NO_3)_3 + C_2H_6N_4O_2 \xrightarrow[\text{Water}]{} Zn_{1-x}Eu_xO + \text{gaseous products} \quad -- (1)$$

.

The detailed flow chart for combustion synthesis is given in Fig.1.

2.2. Instruments used

The powder X-ray diffraction (PXRD) studies were carried out using Phillips X-ray diffractometer (model PW 3710) with Cu Kα radiation (λ=1.54056 Å). The surface morphology of the samples was examined using Scanning electron microscopy (SEM) (JEOL JSM 840A). Transmission Electron Microscopy (TEM) analysis was performed on a Hitachi H-8100 (accelerating voltage up to 200kV, LaB_6 filament) (Kevex Sigma TM Quasar, USA). The UV-Vis spectrum was recorded on a UV-3101 Shimadzu Visible spectrophotometer. The photoluminescence (PL) studies were carried out using a Perkin–Elmer LS-55 luminescence spectrophotometer equipped with Xe lamp. The synthesized samples were irradiated with different doses of γ-rays in the range 1-10 kGy from Co-60 source at room temperature. After the desired exposure, TL glow curves were recorded on a Nucleonics TLD reader taking 5 mg of the sample each time at a heating rate of20^0Cs^{-1}. The EPR spectrum was recorded at room temperature using a JEOL-FE-1X EPR spectrometer operating in the X-band frequency (≈ 9.205 GHz) with a field modulation frequency of 100 kHz. The magnetic field was scanned from 0 to 500 mT and the microwave power used was 10 mW. A powdered specimen of 100 mg was taken in a quartz tube for EPR measurements.

3. Results and Discussion

3.1. Powder X-ray diffraction (PXRD)

Fig.2 shows the powder X-ray diffraction (PXRD) profiles of as-formed undoped and Eu doped ZnOnano powder. The diffraction peaks corresponding to (1 0 0), (0 0 2), (1 0 1), (1 0 2), (1 1 0), (1 0 3), (1 1 2) and (2 0 0) directions have been indexed (JCPDS 36-1451) and found to be in hexagonal wurtzite structure. No other impurity peaks are detected which indicate the presence of ZnO nanocrystals without any amorphous component and other additional Eu_2O_3 crystalline phase. Thus the wurtzite structure is not modified by the addition of Eu into the ZnO matrix. It is clear that the formed ZnO:Eu is in singular phase, its formation is complete at the furnace temperature and further calcination treatment was not necessary. The average crystallite size (D) was estimated from the Debye–Scherrer's equation given by

$$D = \frac{0.9\lambda}{\beta \cos\theta} \qquad \text{..... (2)}$$

where λ represents the wavelength of the X-ray radiation, β is the full width at half maximum (FWHM) of diffraction peak (in rad) and θ is the scattering angle. The crystallite size calculated for Eu doped sample (35 nm) was found to be less when compared to undoped ZnO (39 nm).

The accurate unit cell parameters of undoped ZnO and Eu doped ZnO were determined by Rietveld refinement of the observed diffraction profiles using *FullProf* software [19]. The pseudo-voigt peak profile function was used in order to fit the several parameters to the data point: one scale factor, one zero shifting, four back ground, three cell parameters, five shape and width of the peaks, one global thermal factor and two asymmetric factors. The fitted and observed data along with the difference

between them are shown in the Fig.3. The obtained reliability factors R_p, R_{wp}, R_{Bragg}, χ^2 , R_F and lattice parameters calculated from the Rietveld refinement are tabulated in the Table.1. Lattice parameters, *a* (3.256 Å) and *c* (5.216 Å) and *c/a* ratio (1.602) obtained by refinement show typical values of wurtzite type structure of ZnO. Both samples crystallize in wurtzite hexagonal structure with space group P63mc.Very little change was found in the lattice parameters of undoped and Eu doped ZnO which may be due to low doping concentration of Eu in the ZnO matrix.

3.2. Scanning and Transmission electron microscopy (SEM &TEM)

The morphology of undoped and Eu doped ZnOsamples as obtained by SEM are shown in Fig.4. It can be clearly observed from low resolution SEM that the powder shows many agglomerates with an irregular morphology (4a and 4c). Such a shape is believed to be formed because of the nonuniform distribution of temperature and mass flow in the combustion flame. During the combustion process, gaseous products are evolved and hence the combustion product is more porous as shown in the micrographs. Further higher magnification SEM images (4b and 4d) show the presence of several small particles which is an inherent feature of combustion process. Fig.5 depicts the TEM image of Eu doped ZnO particles which are quasi-hexagonal in shape having average size in the range of ~ 40 nm. This was also confirmed by Debye–Scherrer's equation. Selective area electron diffraction (SAED) (Inset of Fig.5) showed that the nanoparticles are crystalline in nature.

3.3. UV-Visible absorption and band gap measurements

The UV-Vis absorption spectra of undoped and Eu doped ZnO sample is shown in Fig.6. A broad absorption band at ~375 nm was observed in the spectra which is a

characteristic band for the wurtzite hexagonal pure ZnO. A blue shift in the absorption edge is observed in Eu doped ZnO. This shift is perhaps due to band structure deformation caused by the incorporation of Eu in the ZnO lattice. The optical energy gap (E_g) of un-doped and Eu doped ZnO was estimated using the Tauc relation [20]

$$\alpha(h\upsilon) \sim (h\upsilon - E_g)^{1/2} \qquad \ldots\ldots\ldots (3)$$

where $h\upsilon$ is the photon energy and α is the optical absorption coefficient near the fundamental absorption edge. The E_g of undoped and Eu doped ZnO is found to be ~3.178 eV and ~3.395 eV respectively (Inset of Fig.6).

3.4. Photoluminescence (PL) studies

In order to confirm the charge state (+2, +3) of Eu ions present in the sample, PL measurements have been carried out at different excitation wavelengths (254, 325, 488 nm). "The 488 nm photon is in resonance with the $^7F_2 \rightarrow {}^5D_2$ transition of Eu^{3+} ions due to stark splitting effect. The electron can transfer from $^5D_2$ state to $^5D_0$ state by the non-radiative process of excited Eu^{3+} ions, later the electrons population on $^5D_0$ state transfer to 7Fj state of Eu^{3+}".[21]

Fig.7a shows PL emission spectrum at 254 nm excitation. The emission peaks are observed in the blue (420, 445, 457, 484 nm), green (528 nm) and red (600 nm) regions. The peaks at 420 and 457 nm corresponds to the 5d → 4f transitions of Eu^{2+} ion [22,23]. Upon 325 nm excitation (Fig.7b), emission peaks in the range 423 to 484 nm are noticed which are related to Eu^{2+} ions. No intra- 4 f^6 Eu^{3+} related emission is observed which is probably related to the shielding effect due to the existence of the Eu_{Zn}* level [23]. Thus 325nm excitation is not in resonance with any transitions of Eu^{3+} ions.

Further, emission spectrum for excitation 488nm (Fig.7c) consists of two main peaks centered at 586 and 652 nm which are attributed to $^5D_0 - ^7F_1$ and $^5D_0 - ^7F_3$ transitions respectively [24, 25]. The emission at 586 nm originates from the magnetic dipole allowed transition, indicating that Eu^{3+} ions occupy a site with inversion symmetry. The emission spectra of Eu^{3+} generally consist of sharp lines from 550 to 750nm, corresponding to the f–f transitions. The 488 nm excitation is in resonance with the $^7F_2 \rightarrow ^5D_2$ transition of Eu^{3+} ions considering the Stark splitting effect. The 4f–4f emissions of the doped Eu^{3+} ions could be observed when the Eu^{3+} ions were excited at wavelengths that were resonant with their 4f–4f transitions. It can be concluded from PL spectra that these band spectral properties are the characteristic of both Eu^{2+} and Eu^{3+}. However, a very weak emission of Eu^{3+} ions could be observed from the emission spectra. Therefore, it can be concluded that Eu^{2+} and Eu^{3+} ions coexist in the sample. In order to get definite proof for the presence of Eu^{2+} ions, EPR analysis was performed on Eu-doped sample.

3.5. Electron paramagnetic resonance (EPR) studies

The EPR spectrum of ZnO:Eu nanopowder is shown in Fig.8. The EPR spectrum exhibits a broad resonance signal at g = 4.195 the most intense one which is arrtributed to Eu^{2+} ions. The shape of the EPR spectrum of Eu^{2+} ions strongly depends on the relative magnitude of microwave frequency and crystal field strength. The ground state of the Eu^{2+} free ion is 8-fold degenerate. The strong crystal field splits the free ion level into four doubly degenerate energy levels. The Zeeman field removes such remaining degeneracy. As a result of transitions of unpaired electrons between these split levels, additional spectral lines of $g >> 2.0$ and $g < 2.0$ are observed. In addition to the resonance

signal at g = 4.195, we have also observed an intense sharp resonance signals at g = 1.994 and g ~ 2.007 along with additional broad resonance signals at g = 2.540, g = 2.145 and g = 1.775. As ZnO is known to process several intrinsic defects, in order to confirm these additional resonances the authors have performed EPR study of undoped ZnO. It is observed that undoped ZnO showed all the resonance signals except g = 4.195. Therefore, the g = 4.195 signal is assigned to Eu^{2+} which is present in the sample. Our PL results also cofirm the presence of Eu^{2+} in ZnO.

The number of spins participating in resonance at g = 4.195 can be evaluated using the expression given by Weil et al. [26], which includes the experimental parameters of both sample and standard.

$$N = \frac{A_x\,(Scan_x)^2\,G_{std}\,(B_m)_{std}\,(g_{std})^2\,[S\,(S+1)]_{std}\,(P_{std})^{1/2}}{A_{std}\,(Scan_{std})^2\,G_x\,(B_m)_x\,(g_x)^2\,[S\,(S+1)]_x\,(P_x)^{1/2}}\,[Std] \quad , \ldots\ldots\ldots (4)$$

where A is the area under the absorption curve which can be obtained by double integrating the first derivative EPR absorption curve, Scan is the magnetic field corresponding to unit length of the chart, G is the gain, Bm is the modulation field width, g is the g factor, S is the spin of the system in its ground state. P is the power of the microwave source. The subscripts 'x' and 'std' represent the corresponding quantities for ZnO:Eu and the reference ($CuSO4.5H_2O$) respectively. The number of Eu^{2+} ions participating in resonance at room temperature for the studied sample is found to be 2.72 × 1019.

The existence of several resonance signals clearly indicates that several kinds of defects are present in the ZnO:Eu sample. The resonance signals at g = 1.994 and g ~ 2.007 are sharp. These signals are close to free electron value (g = 2.0023) is generally attributed to an unpaired electron trapped on an oxygen vacancy site [27, 28]. The resonance signals at g = 2.145 have been attributed to Zn vacancy. The origin of other signals at g = 2.540 and g = 1.775 is not known.

3.6. Thermoluminescence (TL) studies

Fig.9 shows the variation of TL intensities for ZnO:Eu nanocrystalline phosphors with temperature for different doses (1-10kGy) at a linear heating rate 6 $^{o}Cs^{-1}$.A single glow curve with peak at ~ 355 ^{o}C was recorded in the entire range of irradiated samples. The results are in good agreement with literature [29]. It is observed that, the TL intensity increases with γ-ray dose up to 6 kGy and then it decreases with further increase in dose (8-10kGy) (Fig.10). This increase in intensity can be explained on the basis of track interaction model (TIM) [30, 31]. This model suggests that the number of generated traps as a result of irradiation depends on both the cross section of the tracks and the length of the tracks in the matrix. In nano materials, the length of such a track may be few tens of nano meters, so the number of trap centres / luminescence centres will be less for lower doses than their microcrystalline form.

However, if we increase the irradiation dose, more overlapped tracks occur that may not give extra TL, as a result of which saturation occurs. But in case of nanomaterials, there still exist some particles that would have been missed while being targeted by high energy radiation due to very tiny size. Thus on increasing the dose, these nanoparticles which had earlier been left out from the radiation interaction, now

generates trapping and luminescence centers. Thus we do not get saturation in nano materials even at higher doses. However, further higher doses result in saturation or decrease in the TL intensity due to the same reason of overlapping of tracks. This may further be explained in terms of high surface to volume ratio which results in high surface barrier energy for nanomaterials. Thus on increase in dose, the energy density crosses the barrier and a large number of defects are produced in the nanomaterials which ultimately keep on increasing with the dose till saturation is achieved.

Secu et al [29] have studied TL of ZnO nano needle arrays and films and observed nano needles show a broad and composite peak at ~360 ^{0}C and its intensity decreases with the anodizing time. The shape of the TL glow curves of nano needles and films are very similar indicating that, the physical properties of the traps are almost same. TL is mainly due to the recombination of charge carriers released from the surface traps associated with the interstitial oxygen ion. Further, polycrystalline ZnO show TL peak at ~380 ^{0}C with a shoulder at lower temperature. The TL curve is similar to that one recorded for ZnO nano needles except for a small shift towards higher temperature. This might suggest a linkage of the defects and TL mechanism. Indeed oxygen related defect sites as singly occupied oxygen vacancies (isolated or associated to the other impurities or defect sites) or vacancy- interstitial pairs have been observed.

Mustafa Oztas [32] studied ZnO:Cu nanoparticles prepared by the spray pyrolysis method irradiating using a ^{90}Sr/^{90}Y β-source (2.27 MeV) at a dose rate of 0.015 Gy/s at room temperature. Two characteristic glow peaks at 117 ^{o}C and 196 ^{0}C were observed. The TL intensity increases with decreasing annealing temperature and particle size. The TL enhancement may be caused by the recombination of carriers released from

the surface states by heating. Smaller particles have higher surface / volume ratio and more surface states, therefore contain accessible carriers for TL. Besides, the carrier recombination rate increases with decrease in size of the particles and annealing temperature. Sahu et al [33] studied TL of ZnOnanopowder by sonication method irradiating with β-rays at heating rate $5^0C\ s^{-1}$. The material prepared in pulsed mode show three peaks 125 ^{0}C (well resolved) along with shouldered peaks at 330 ^{0}C and 275 ^{0}C. However in continuous mode method, two well resolved glow peaks at 125 ^{0}C and 290 ^{0}C were observed. Further, the glow peak intensity is increased more than 10 times than that of pulsed mode.

The determination of kinetic parameters has been an active area of research and various techniques have been developed over the time to derive these parameters from the glow curve. The TL glow curve for the synthesized ZnO:Eu sample (Fig.11) have single broad peak without any Inflection points indicating the presence of other overlapped peaks. However, if we apply peak shape method for the whole experimental glow curve and evaluate the parameters, it is found that the geometrical factor is equal to 0.511 which seems to be bit unrealistic since its value lies in between 0.42 and 0.52. The unexpected value of geometrical factor led us to speculate that this peak may be comprised of more than one peak having a close distribution of their trap depths, which are superimposed giving rise to broad TL glow peaks. This prompted us to make use of curve fitting technique to analyze the glow curve. For analyzing the TL glow curve in which we firstly did deconvolution based on Gaussian function and then analysed the individual deconvoluted peaks using Chen's set of empirical formulae [34] for the peak

shape method as summarized below. The evaluated trapping parameters E and b were then used as the initial parameters in kinetic equations.

The activation energy (*E*)

$$E_\alpha = c_\alpha\left(\frac{kT^2{}_m}{\alpha}\right) - b_\alpha\left(2kT_m\right) \qquad \ldots\ldots\ldots (5)$$

Where $\alpha = \tau, \delta, \omega$ with $\tau = T_m - T_1$, $\delta = T_2 - T_m$, $\omega = T_2 - T_1$

$$C_\tau = 1.51 + 3.0\left(\mu_g - 0.42\right), \quad b_\tau = 1.58 + 4.2\left(\mu_g - 0.42\right)$$

$$C_\delta = 0.976 + 7.3\left(\mu_g - 0.42\right), \; b_\delta = 0 \qquad \ldots\ldots\ldots (6)$$

$$C_\omega = 2.52 + 10.2\left(\mu_g - 0.42\right), \; b_\omega = 1$$

The geometrical form factor (symmetry factor):

$$\mu_g = \frac{T_2 - T_m}{T_2 - T_1} \qquad \ldots\ldots\ldots (7)$$

The obtained peak parameters are listed in Table 2. The average activation energy (*E*) of ZnO: Eu was found to be in the range 0.21-1.26 eV. This wide range might be due to the extension of the band gap of ZnO:Eu nanocrystalline material, which has been observed in several nanomaterials [35].

4. Conclusions

The ZnO: Eu (1mol %) nanopowders were synthesized through a low-temperature solution combustion method using ODH fuel. Hexagonal wurtzite structure without secondary phase was observed from XRD results. Scanning electron microscopy (SEM) and transmission electron microscopy (TEM) studies reveal particles are agglomerated with quasi-hexagonal morphology. Photoluminescence (PL) emission under 254 nm excitation show peaks in regions blue (420-484 nm), green (528 nm) and

red (600 nm) which corresponds to both Eu^{2+} and Eu^{3+} ions. Further, with the increase of excitation wavelength to 488 nm, the emission peaks at 586 and 652 nm are observed which are due to $^5D_0 \rightarrow ^7F_1$ and $^5D_0 \rightarrow ^7F_3$ transitions of Eu^{3+} ions respectively. The EPR spectrum exhibits a broad resonance signal at g = 4.195 the most intense one which is arrtributed to Eu^{2+} ions. The resonance sharp signals at g = 1.994 and g ~ 2.007 are attributed to an unpaired electron trapped on an oxygen vacancy site. The resonance signals at g = 2.145 have been attributed to Zn vacancy. TL studies on ZnO: Eu nanocrystalline phosphor was studied with γ- irradiation for a dose range 1-10kGy at a linear heating rate 6 $^oCs^{-1}$. A broad glow curve with peak at ~ 355 ^oC was recorded in the entire range of irradiated samples. The kinetic analysis of the experimental TL glow curve was carried out using Chen's peak shape method and the average activation energy was found to be in the range 0.21-1.26 eV.

References

[1] A.B. Djurisic, A.M.C. Ng, X.Y. Chen,*Prog. Quantum Electron*. 34 (2010) 191–259.

[2] U.Ozgur, Y. I.Alivov, C.Liu, A.Teke, M. A. Reshchikov, S.Dogan, V.Avrutin, S. J.Cho, H.Morkoc, *J ApplPhys* 98(2005)041301-041305.

[3] Yunxin Liu, ChangfuXu, Qibin Yang, *J. Appl. Phys.*105(2009)084701-084706

[4] K.Nomura, H.Ohta, K.Ueda, T.Kamiya, M.Hirano, H.Hosono, *Science*300 (2003)1269-1272.

[5]R.N.Bhargava , V.Chhabra , T.Som , A.Ekimov, N.Taskar , *Phys.StatusSolidi* B 229(2 002) 897-901.

[6] K. Machida, G. Adachi, J. Shiokawa, *J. Lumin.* 21 (1979) 101-106.

[7] Z.W. Pei, Q. Su, J.Y. Zhang, *J. Alloys Compd.* 198 (1993) 51-55.

[8] T. Rattana, S. Suwanboon, P. Amornpitoksuk, A. Haidoux, P. Limsuwan, J. Alloys and Compounds 480 (2009) 603–607

[9] Julie De Merchant , Michael Cocivera, *Chem. Mater.* 7 (1995),1742–1749

[10] Paul O'Brien, Tahir Saeed, Jonathan Knowles, *J. Mater. Chem*. 6 (1996)1135-1140.

[11] Y.Yang, H.Chen, B.Zhao, X.Bao, *J. Cryst. Growth*, 263 (2004)447-453.

[12] Bin Liu, Hua Chun Zeng, *J. Am. Chem. Soc.*, 125 (15)(2003) 4430–4431.

[13] SubhashThota, TitasDutta, Jitendra Kumar, *J. Phys.: Condens. Matter* 18(2006)2473-2478

[14] Zhijian Wang, Haiming Zhang, Ligong Zhang, Jinshan Yuan, Shenggang Yan, Chunyan Wang, *Nanotechnology*,14 (2003) 11-15.

[15] C.Cruz-Vázquez, V. R.Orante-Barrón, H.Grijalva-Monteverde, V. M.Castaño, R.Bernal, Mater Lett. 61(2007)1097-1100.

[16] C. Cruz-Vázquez, R. Bernal, S. E.Burruel-Ibarra,H. Grijalva-Monteverde, M.Barboza-Flores, Optical Mater. 27(2005)1235-1239.

[17] A. K.Srivastava, K.Ninagawa, S.Toyoda, B. R.Chakraborty, S.Chandra, Opt. Mater. 32(2009)410-413.

[18] S. Ekambaram, K. C.Patil, J. Alloys and Compounds, 24(1997) 7-12.

[19] Rodriguez-Carvajal J, (2009) Fullprof.2000: A program for Rietveld, Profile matching and integrated intensity refinements for X-ray and neutron data. Version 1.6.Laboratoire Leon, Brillouin, Gifsuryvette, France.

[20] H. Nagabhushana, B. M.Nagabhushana, Madesh Kumar, H. B.Premkumar, C.Shivakumara, R. P. S.Chakradhar, Phil. Mag.26(2010)3567-3579.

[21] Mingya Zhong, Guiye Shan, Yajun Li, Guorui Wang, Yichun Liu, Mater. Chem. Phys. 106 (2007) 305–309

[22] S.S. Ashtaputre, A.Nojima, S. K.Marathe, D. Matsumura, T.Ohta, Tiwari R, G. K.Dey, S. K.Kulkarni, J. Phys. D: Appl. Phys.41(2008)015301-015306.

[23] Camellia Panatarani, I. WuledLenggoro, Kikuo Okuyama, J. Phy. Chem. Solids, 65(2004) 1843-1847.

[24] P. M.Aneesh, M. K.Jayaraj, Bull. Mat. Sci. 33(2010)227-231.

[25] L. Robindro Singh, R. S.Ningthoujam, V. Sudarsan, S. Dorendrajit Singh, S. K.Kulshreshth, J. Lumin. 128 (2008)1544-1550.

[26] J. A. Weil, J. R. Bolton and J. E. Wertz, (1994) Electron Paramagnetic Resonance-Elementary Theory and Practical Applications, Wiley, New York, p.498.

[27] Yu B, Zhu C, Gan F, Huang Y, *Mater. Lett*. 33 (1998) 247-250.

[28] Liqiang Jing , ZiliXu , Jing Shang, Xiaojun Sun, WeiminCai, HaichenGuo, Mater. Sci. Eng. A, 322(2002)356-361.

[29] C. E.Secu, Mariana Sima, Opt. Mat. 31(2009)876-880.

[30] Y.S. Horowitz, O. Avila, M. Rodriguez-Villafuerte, Nucl. Instr. Meth. Phys. Res. B 184 (2001) 85-112.

[31] S Mahajna, Y S Horowitz J. Phys. D: Appl. Phys. 30 (1997) 2603-2619.

[32] Mustafa Oztas, J. Mater. Sci: Mater Electron 17(2006)937-941.

[33] DojalisaSahu, B. S.Acharya, B. P. Bag, T. H.BasantaSingh, R. K.Gartia, J. Lumin. 130(2010)1371-1378.

[34] K. R.Nagabhushana, B. N.Lakshminarasappa, Fouran Singh,Radiat. Meas. 43(2008) S651-S655.

[35] N. Salah, P. D.Sahare, A. A.Rupasov, *J. Lumin*. 124(2007) 357–364.

Table Captions

Table.1 Reliability factors and lattice parameters calculated from the Rietveld refinement

Table.2 Kinetic parameters of ZnO:Eu obtained using glow curve shape method

Figure Captions

Fig.1 Flowchart for the synthesis of combustion derived ZnO:Eu

Fig.2 PXRD patterns of undoped and Eu doped ZnO

Fig.3 Experimental and simulated diffraction pattern with Rietveld refinement using FullProf of (a) ZnO and (b) Eu doped ZnOnanopowders

Fig.4 SEM images of undoped (a & b) and Eu doped (c & d) ZnO nanopowders

Fig.5 TEM image of Eu doped ZnO nanopowder (Inset) SAED pattern

Fig.6 UV-Vis spectra of undoped and Eu doped ZnO nanopowders [Inset: Plot of $(\alpha h\upsilon)^2$vs $(h\upsilon)$]

Fig.7 PL emission spectrum of Eu doped ZnO (a) λ_{exi} = 254 nm (b) λ_{exi} = 325 nm (c) λ_{exi} = 488 nm

Fig.8 EPR spectrum of Eu doped ZnO nanopowder

Fig.9 TL glow peaks of ZnO:Eu at different γ-ray doses

Fig.10 Variation of TL intensity of ZnO: Eu with gamma irradiation

Fig.11 A typical glow curve for ZnO:Eu nanocrystalline phosphor after 10kGy gamma exposure at a heating rate of 6 $^0Cs^{-1}$. Dotted lines represent the deconvoluted peaks

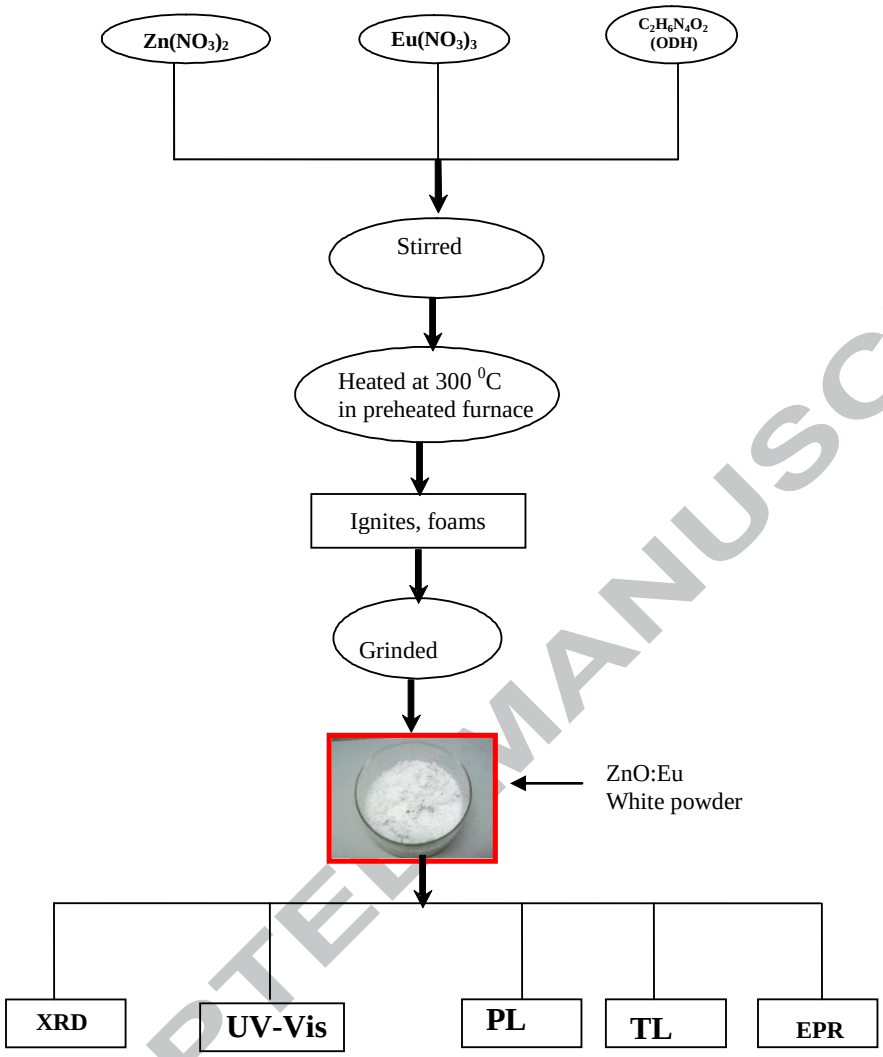

Fig.1 Flowchart for the synthesis of combustion derived ZnO:Eu

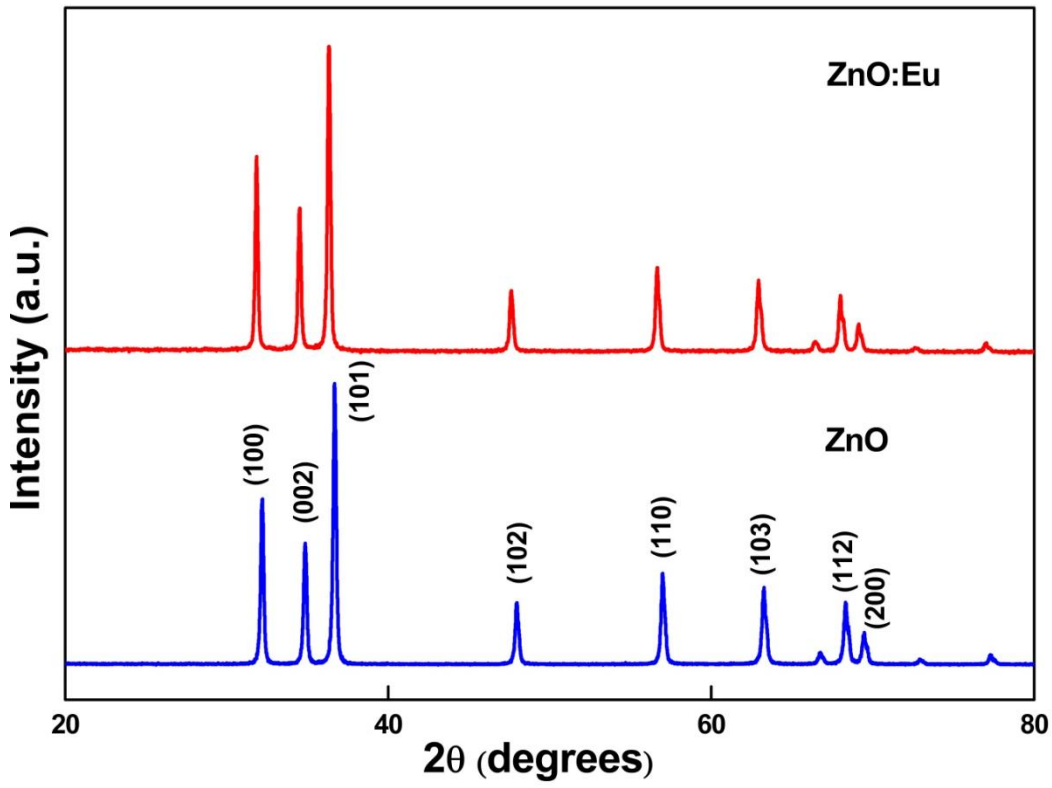

Fig.2 PXRD patterns of undoped and Eu doped ZnO

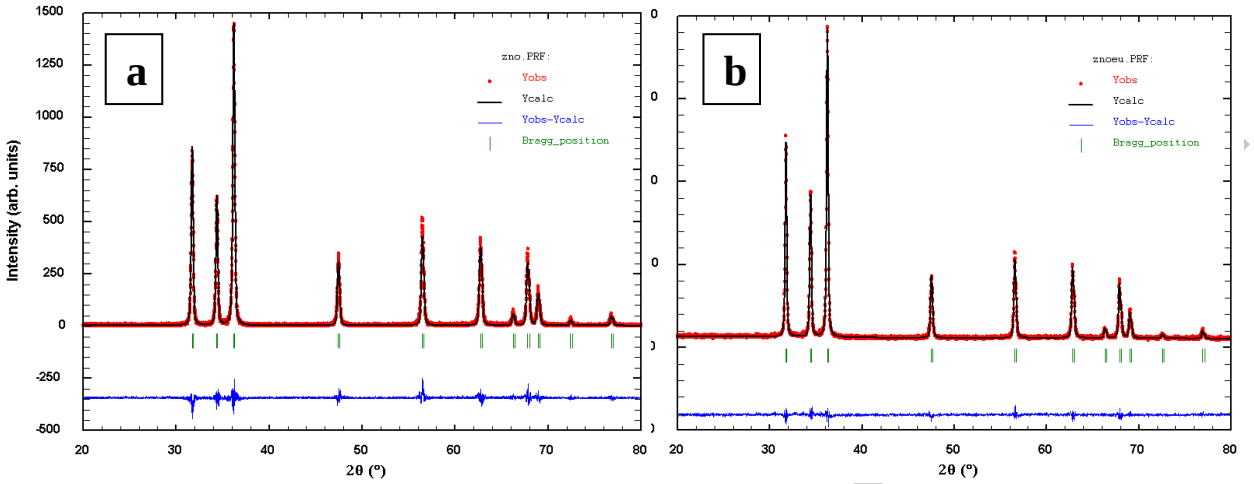

Fig.3 Experimental and simulated diffraction pattern with Rietveld refinement using FullProf of (a) ZnO and (b) Eu doped ZnO nanopowders

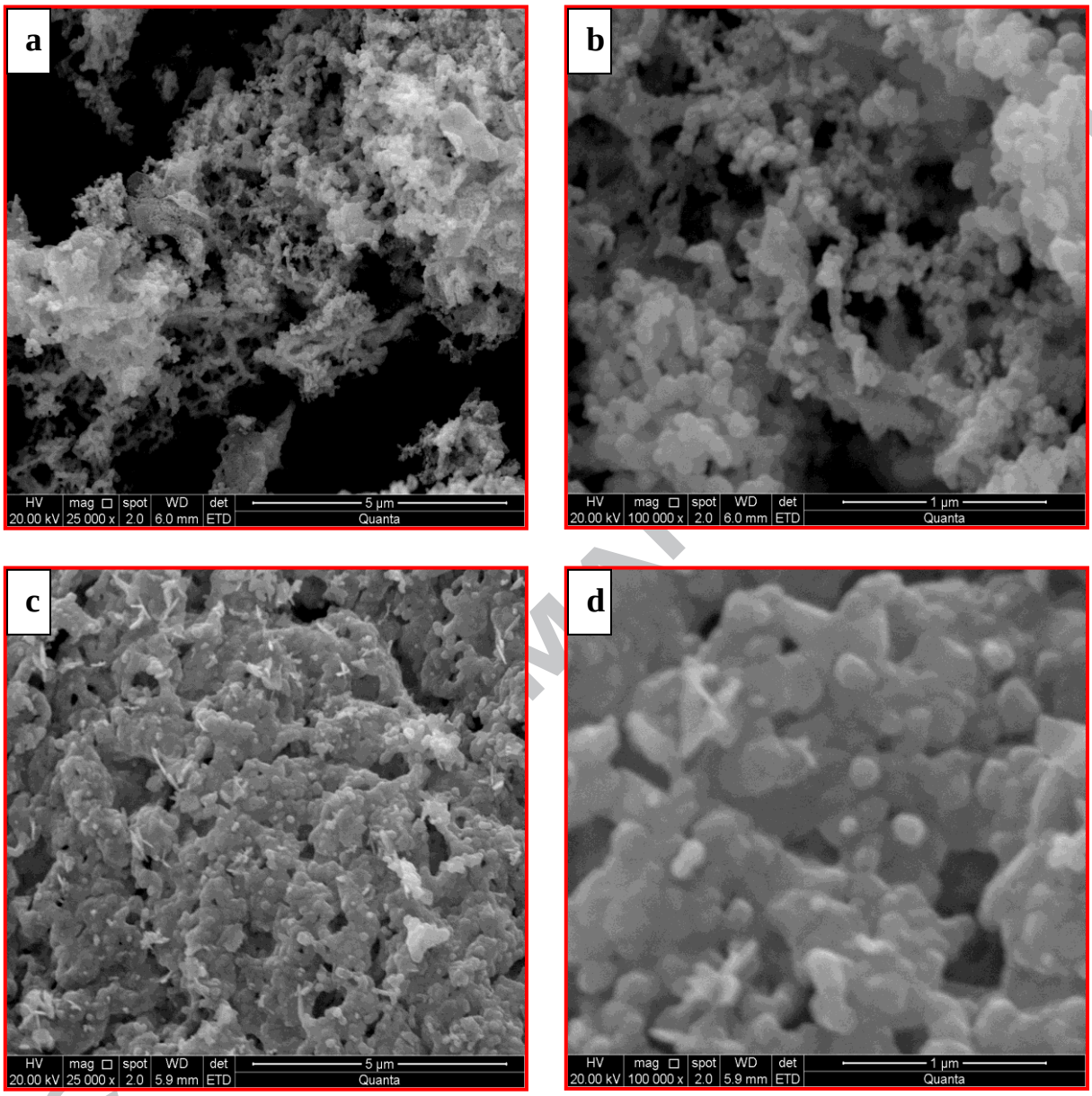

Fig.4 SEM images of undoped (a & b) and Eu doped (c & d) ZnO nanopowders

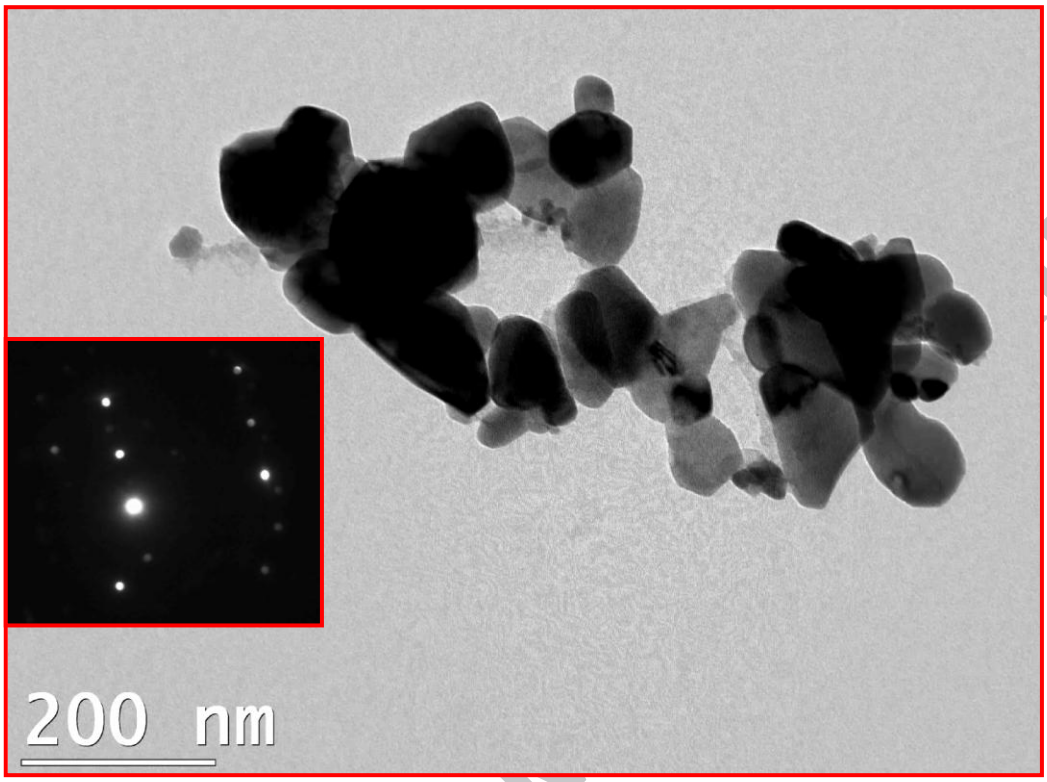

Fig.5 TEM image of Eu doped ZnO nanopowder (Inset) SAED pattern

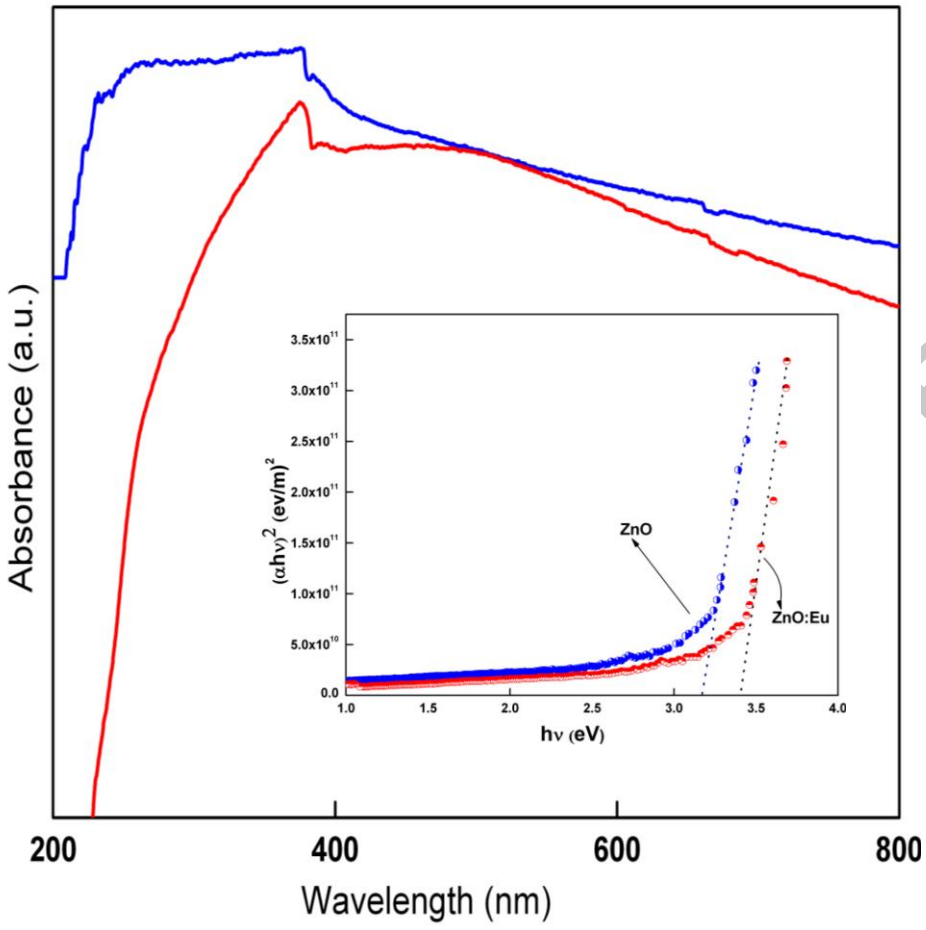

Fig.6 UV-Vis spectra of undoped and Eu doped ZnO nanopowders

[Inset: Plot of $(\alpha h\upsilon)^2$ v/s $(h\upsilon)$]

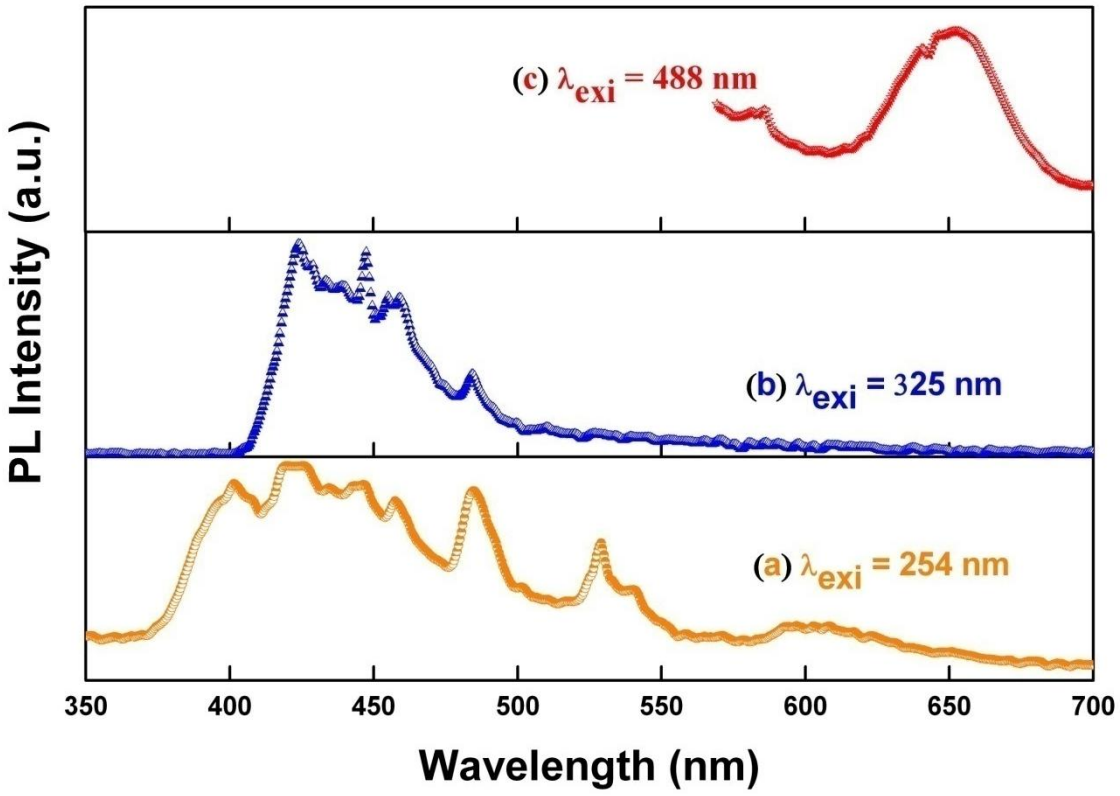

Fig.7 PL emission spectrum of Eu doped ZnO (a) λ_{exi} = 254 nm (b) λ_{exi} = 325 nm (c) λ_{exi} = 488 nm

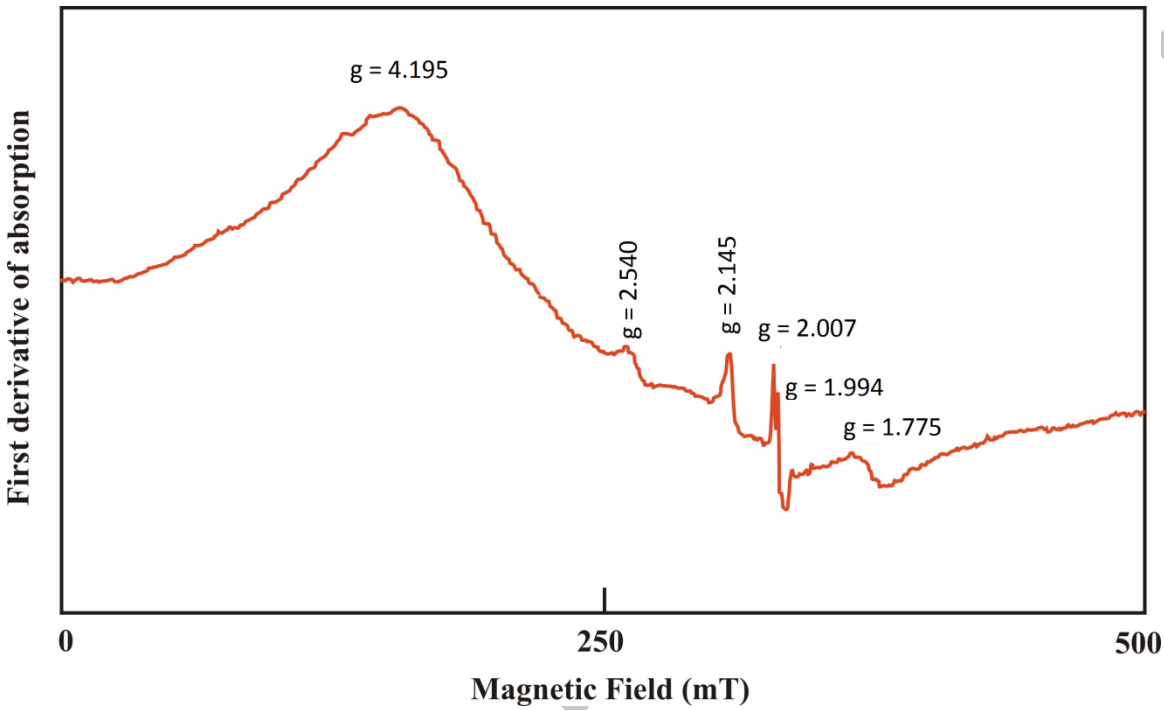

Fig.8 EPR spectrum of Eu doped ZnO nanopowder

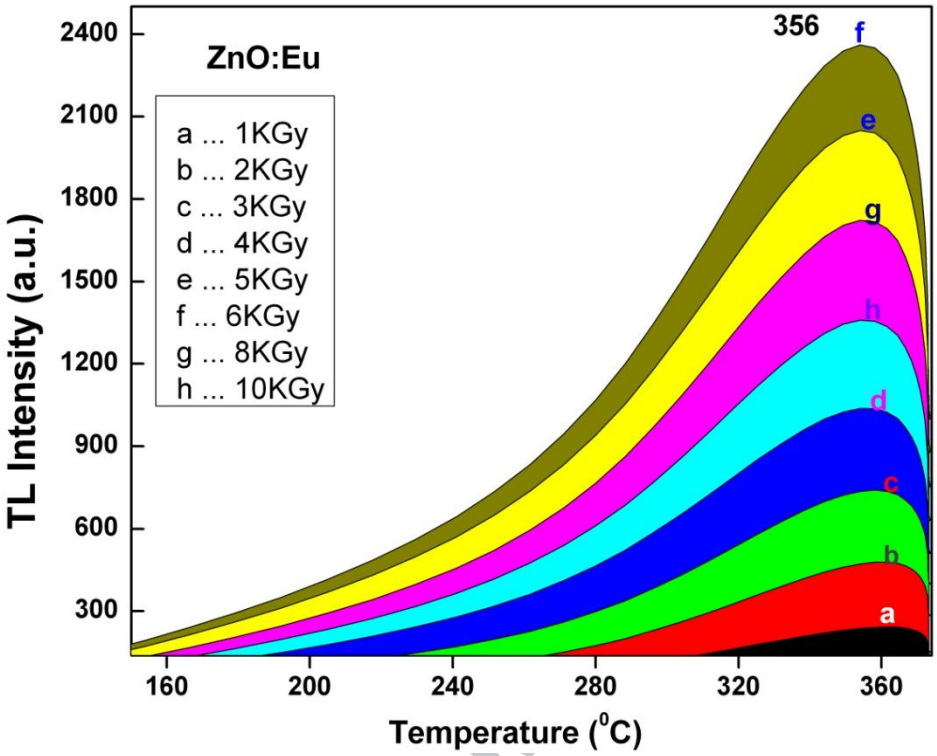

Fig.9 TL glow peaks of ZnO:Eu at different γ-ray doses

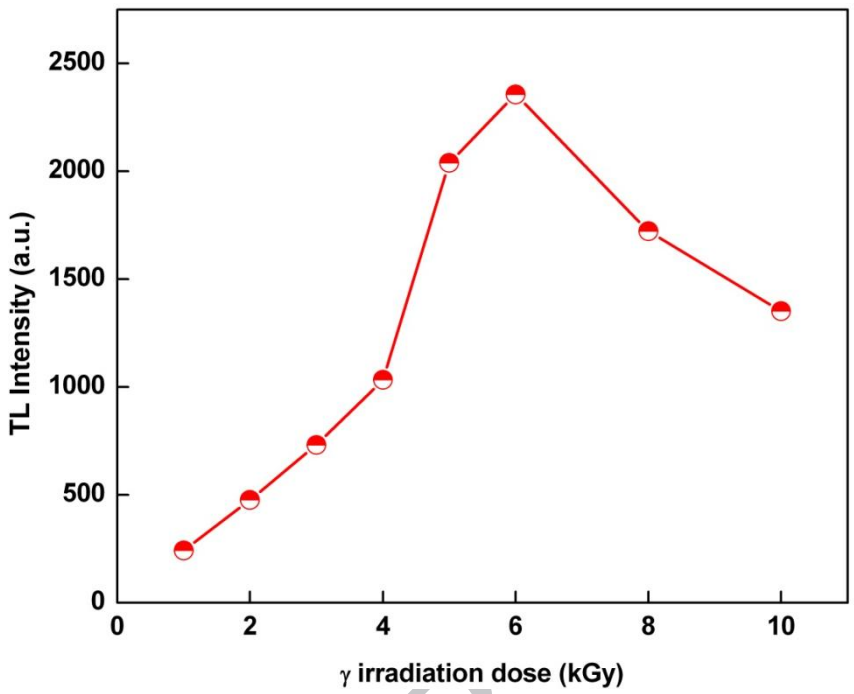

Fig.10 Variation of TL intensity of ZnO: Eu with gamma irradiation

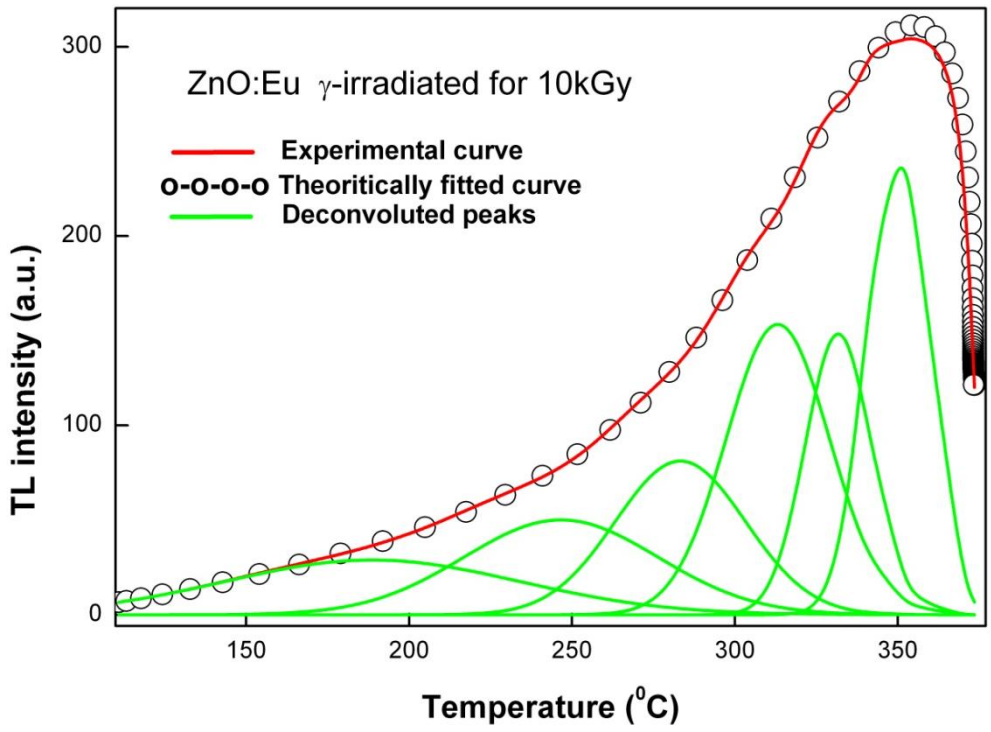

Fig.11 A typical glow curve for ZnO:Eu nanocrystalline phosphor after 10kGy gamma exposure at a heating rate of 20 $^{0}Cs^{-1}$. Dotted lines represent the deconvoluted peaks

Table.1 Reliability factors and lattice parameters calculated from the Rietveld refinement

Sample	Lattice parameters (Å)		Volume of unit cell $(Å)^3$	R_p	$R_{\omega p}$	χ^2	R_{Brag}	R_f
	a	c						
ZnO	3.256(1)	5.216(2)	47.91(3)	12.4	20.9	1.18	3.79	2.41
$Zn_{0.999}Eu_{0.001}O$	3.252(2)	5.208(3)	47.71(1)	6.69	9.35	0.860	2.31	1.88

Table.2 Kinetic parameters of ZnO: Eu obtained using glow curve shape method

Deconvol-uted peaks	T_m (^oC)	Order of Kinetics (b)	Activation Energy (eV)				Frequency factor (s) s^{-1}
			E_τ	E_δ	E_ω	E_{Avg}	
1	246	2	0.1879	0.2400	0.2141	0.2140	1.99×10^4
2	283	2	0.3978	0.4403	0.4204	0.4195	3.58×10^7
3	313	2	0.6878	0.7036	0.6993	0.6969	2.93×10^{11}
4	332	2	1.1575	1.1453	1.1600	1.1543	8.75×10^{17}
5	351	2	1.2636	1.2503	1.2674	1.2604	3.33×10^{18}

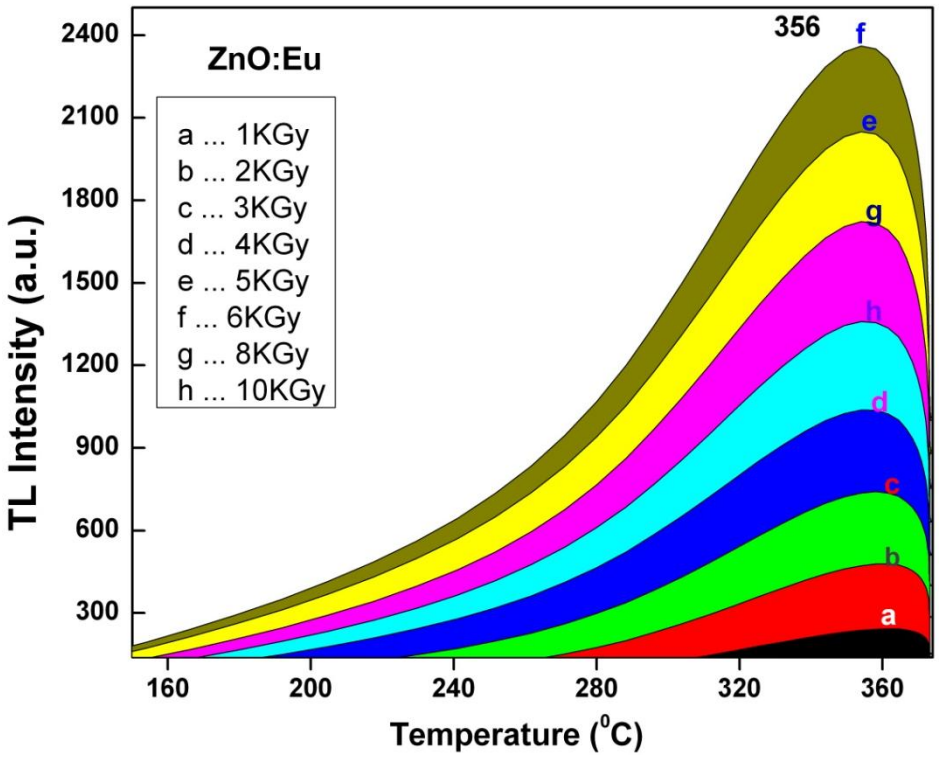

Research Highlights

- ZnO:Eu nanopowders have been synthesized by simple low cost SCS method.
- SEM and TEM images reveal quasi-hexagonal morphology of the samples.
- ZnO:Eu nanopowders show PL peaks corresponding to both Eu^{2+} and Eu^{3+} ions.
- EPR spectrum exhibits a broad resonance signal attributed to Eu^{2+} ions.
- EPR and TL studies reveal native defects. The trap parameters are discussed.